Electrical Conductivity in Soils: Underlying Phenomena

Katherine A. Klein[1] and J. Carlos Santamarina[2]
[1]Assistant Professor, Department of Civil Engineering, University of Toronto,
Toronto, Ontario, M5S 1A4, Canada
[2]Professor, Department of Civil and Environmental Engineering, Georgia Institute of Technology,
Atlanta, Ga 30332 U.S.A.
Email: klein@ecf.utoronto.ca

ABSTRACT

Electrical conductivity can be accurately and readily measured in the laboratory and in the field, with minimal electrode effects even in high specific surface soils and/or high ionic concentration pore fluids. Electrical conductivity combines the contributions of particle conduction, surface conduction and pore fluid conduction, and the effects of particle shape and fabric. The interplay between participating soil parameters is often obscured in typical empirical equations, such as Archie's law. New experimental results show that surface conduction is an important contributor to global soil conduction in high specific surface soils that are saturated with low-ionic concentration pore fluids; the relevance of surface conduction increases with decreasing porosity. On the other hand, pore fluid conduction prevails as the conductivity of the electrolyte and the porosity of the soil increase. Furthermore, low frequency conductivity anisotropy increases with increasing ionic concentration. Simple yet robust microscale analytical models properly capture the observed interplay between the most relevant soil parameters.

Introduction

Soils are porous, multi-phase media consisting of a solid skeleton made of particles, and pores filled with a fluid phase. In most cases, the pore fluid is an aqueous electrolyte. The finer the soil, the higher the specific surface, the wider the range of possible porosities, and the stronger the role of electrical interparticle interactions and fluid-particle interactions on soil behavior. Clay minerals, or phyllosilicates, develop a pH-dependent surface charge because of isomorphic substitution and uncompensated bonds at particle edges (Weaver, 1989; Velde, 1992). The surface charge is balanced by the presence of counterions. When dry, the neutralizing counterions are tightly bound to the surface, and excess ions form salt precipitates. When wet, thermally agitated polar water molecules come in contact with the excess precipitated salt and form the aqueous electrolyte that fills the pores (*i.e.,* free water molecules and hydrated ions). At the same time, water also reaches and hydrates the counterions on the particle surface.

The ionic distribution within the vicinity of the clay particle is determined by thermal agitation and electrostatic forces, rendering a characteristic concentration distribution with high cation and low anion concentrations near the particle, reaching bulk solution concentrations with distance from the surface (typically in the order of 50 to 150 Å—Fig. 1). A layer of tightly bound ions remains near the surface (Stern layer) and a region of diffuse ions follows (Gouy layer). The Stern layer is a few angstroms in thickness and the boundary between the two layers is called the outer Helmholtz plane (Lyklema, 1995). The electrical surface potential of particles cannot be measured directly. However, the net electric potential at the slip/shear plane can be assessed using electrophoretic measurements (Fig. 1). This parameter is the zeta potential, and in simple cases, it is a good approximation for the potential at the outer Helmholtz plane (Lyklema, 1991; Adamson, 1990; Stumm, 1992).

Electromagnetic techniques have been used for more than a century to gain subsurface information such as soil properties (*e.g.,* soil type, porosity, structure, and pore fluid), stratigraphy, and the location of anomalies (*e.g.,* water table, metallic objects, cavities, and contaminants). Field techniques include resistivity profiling (Ward, 1990), magnetometric resistivity (Edwards and Nabighian, 1991), induced polarization (Marshall and Madden, 1959), ground penetrating radar (Daniels and Roberts, 1994), and time-domain reflectometry (Topp *et al.,* 1984). Likewise, laboratory electrical measurements are conducted to characterize soils in view of site exploration, to enhance the understanding of geomaterials, and to gain insight into geoprocesses. Difficulties in low frequency measurements arise due to electrode polarization, which can strongly affect permittivity measurements. However, conductivity measurements are minimally impacted by electrode effects at kHz frequencies and higher (Klein and Santamarina, 1997).

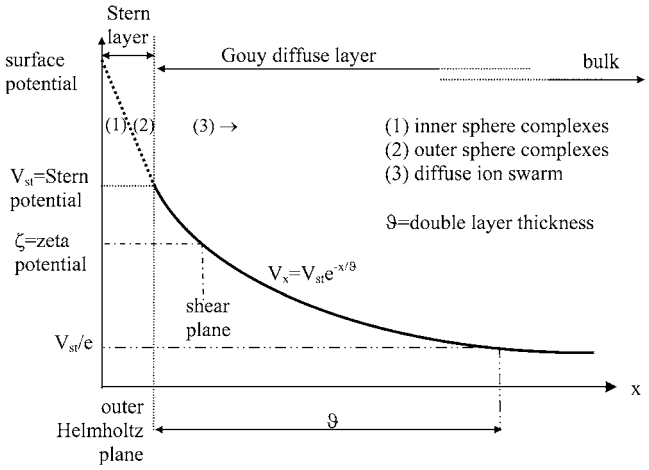

Figure 1. Potential distribution near a mineral surface—the Stern layer and the diffuse double layer.

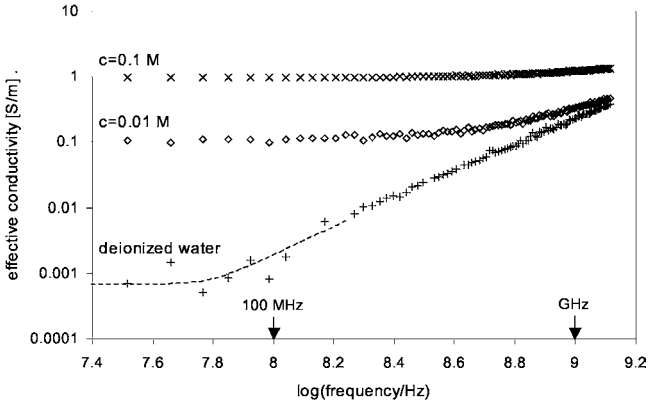

Figure 2. Conduction and polarization losses are evident in the spectral response of effective conductivity for deionized water and NaCl solutions.

Therefore, conductivity measurements provide a robust means for evaluating soil specimens (including their anisotropy) and monitoring the evolution of geo-processes.

Electrical conductivity is a measure of charge mobility in response to an applied electric field. Conduction in wet geomaterials is mainly due to ion migration in the pore space. In addition, ions in the counterion cloud around particle surfaces contribute "surface conduction". The purpose of this paper is to examine soil characteristics that affect the electrical conductivity of fine-grained soils, including ionic concentration, porosity, specific surface and particle orientation, and underlying phenomena such as ion mobility, surface conduction and anisotropy.

Electrical Conductivity in Relation to other Electromagnetic Parameters

The three electromagnetic properties of matter are conductivity σ, dielectric permittivity ε*, and magnetic permeability μ*. The dielectric permittivity and the magnetic permeability are frequency dependent complex quantities consisting of real (ε′ or μ′) and imaginary (ε″ or μ″) components:

$$\varepsilon^* = \varepsilon' - j\varepsilon'' \tag{1}$$

$$\mu^* = \mu' - j\mu'' \tag{2}$$

where $j^2 = -1$ denotes an imaginary number. The imaginary components of permittivity and permeability are measured together with conductivity. Therefore, the measured "effective conductivity" σ_{eff} combines DC conductivity losses with polarization and magnetization losses (Klein and Santamarina, 2000),

$$\sigma_{eff} = \sigma\frac{\mu'}{\mu_o} + \left(\varepsilon'\frac{\mu''}{\mu_o} + \varepsilon''\frac{\mu'}{\mu_o}\right)\omega \tag{3}$$

where ω is angular frequency [rad/s] and $\mu_o = 1.26\cdot10^{-6}$ H/m is the magnetic permeability of free space. The rest of this study assumes that the medium is non-ferromagnetic. In this case, the real and imaginary magnetic quantities are $\mu'/\mu_o = 1$ and $\mu''/\mu_o = 0$, and Eq. 3 reduces to

$$\sigma_{eff} = \sigma + \varepsilon''\omega \tag{4}$$

Fig. 2 shows the spectral response of three aqueous electrolytes. The effective conductivity remains constant at low frequencies. However, as the excitation frequency approaches the orientational polarization of free water (relaxation time $\tau_{rel} = 8.2\cdot10^{-12}$ s), the effective conductivity begins increasing due to polarization losses ε″. The effect is most pronounced in low conductivity electrolytes, however, it is imperceptible when conduction losses prevail with respect to polarization losses in high conductivity electrolytes (*i.e.,* $\sigma \gg \varepsilon''\omega$), in agreement with Eq. 4. (Note: interpretation details can be found in Santamarina *et al.,* 2001).

Electrolyte Conductivity - Ionic Mobility

The conductivity of an electrolyte σ_{el} [S/m] is determined by ionic valence z, concentration c [mol/m^3], and mobility u [m^2/(V·s)]. Then, the contribution of a given ionic species to the conductivity of the electrolyte is (Lyklema, 1991)

$$\sigma_{el} = zcuF = c\Lambda \tag{5}$$

contribution by an ionic species

where F = 96,485.3 C/mol is Faraday's constant and Λ is molar conductivity [Sm^2/mol]. The molar conductivity of the electrolyte is the sum of the molar conductivities of the individual ions. The ionic mobility is defined as the terminal velocity of an ion subjected to a unit electric field

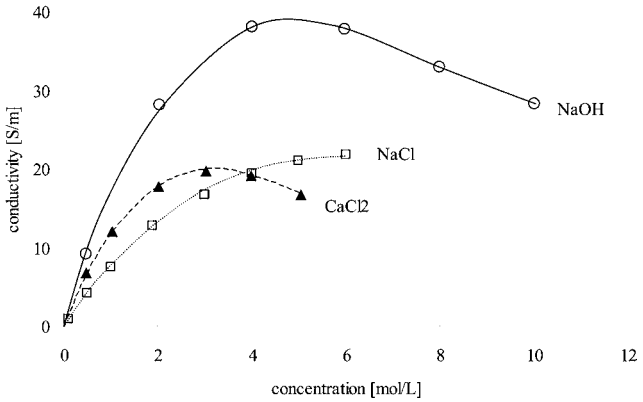

Figure 3. The effect of ionic concentration on electrical conductivity (data in Klein, 1999).

$$u = \frac{v_{ion}}{E} = \frac{ze_o}{6\pi\eta r_h} = \frac{ze_o}{kT}D \tag{6}$$

where v_{ion} is the velocity of the ion [m/s], E is the strength of the electric field [V/m], $e_o = 1.602 \cdot 10^{-19}$ C is the electronic charge, $k = 1.381 \cdot 10^{-23}$ J/K is Boltzmann's constant, T is the absolute temperature [K], D is the diffusion coefficient [m^2/s], r_h is Stokes' radius for the hydrated ion [m], and η is the viscosity of the fluid [Pa·s]. The linear relation captured in Eq. 5 is applicable for low concentration electrolytes where ion-ion interactions are negligible (initial tangent in Fig. 3). An empirical relationship between electrolyte conductivity and ionic concentration for low ionic concentrations at 20°C is (Annan, 1992)

$$\sigma_{el} = 0.15\ TDS \tag{7}$$

where σ is in [mS/m] and TDS is total dissolved salts in [mg/L]. As concentration increases, ionic mobility decreases. Eventually, the decrease in mobility may prevail over the increase in ion availability, and the conductivity of the electrolyte decreases as shown in Fig. 3 for $CaCl_2$ and NaOH solutions.

Temperature also affects the electrical conductivity of an electrolyte. At normal temperatures, ionic mobility and the conductivity of electrolytes increase as temperature increases, as captured in the following empirical relationship (Keller and Frischknecht, 1966)

$$\sigma_{el-T} = [1 + \beta_T(T - 18)]\sigma_{el-18C} \tag{8}$$

where $\beta_T \approx 0.025$/°C, T is the selected temperature in °C ($T < 150$°C), and σ_{el-18C} is the electrolyte conductivity at 18°C. Excessive thermal agitation at very high temperatures can cause a decrease in electrolyte conductivity.

Porosity, Surface Conduction, and Specific Surface

Porosity, specific surface, and pore fluid characteristics affect soil conductivity. The interplay between these

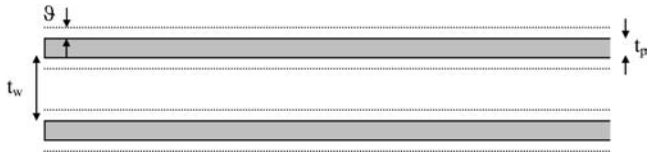

Figure 4. Mixture conductivity parallel to infinitely long platy particles. Particles, electrolyte, and double layers are shown (assumes 100% saturation).

variables is explored in the simple case of infinitely long, parallel, platy particles subjected to an electric field parallel to the particles (Fig. 4). The conductivity of the medium σ_{mix} involves the parallel contributions of the electrolyte conductivity σ_{el} (water layer thickness t_w), the particle conductivity σ_p (thickness of the particles t_p), and the "excess surface charge conduction" λ_{ddl}

$$(\sigma_{mix})_{//} = \frac{\sigma_p t_p + \sigma_{el} t_w + 2\lambda_{ddl}}{t_w + t_p} \tag{9}$$

In this expression, σ_{el} is considered constant across the water layer and the contribution of excess ions near the mineral surfaces is taken into consideration by λ_{ddl}. For flat particles, the particle thickness t_p can be related to the specific surface of the particles S_a and the unit weight of the mineral that makes the particles γ_p,

$$t_p = \frac{2g}{S_a \gamma_p} \tag{10}$$

where g is gravity [m/s^2]. Additionally, the thickness of the water layer t_w is related to the thickness of the particles through the void ratio, $e = t_w/t_p$. Substituting these relations into Eq. 9 renders

$$(\sigma_{mix})_{//} = \frac{\sigma_p + \sigma_{el} e + \lambda_{ddl} \frac{\gamma_p}{g} S_a}{1 + e} \tag{11}$$

The potential at the plane where ions contribute to surface conduction Φ [V] lies between the surface potential and the zeta potential (and it is frequency dependent, as discussed in the following section). If this potential is known, then the surface charge density that corresponds to mobile ions can be determined. At low potentials, the surface charge density ρ can be linearly related to Φ (Lyklema, 1995)

$$\rho_{(est)} = \frac{\Phi \varepsilon'_w}{\vartheta} \quad [C/m^2] \tag{12}$$

and surface conduction is estimated as

$$\lambda_{ddl(est)} = \rho_{(est)} u_{cat} \quad [S] \tag{13}$$

where u_{cat} is the cationic mobility [m^2/(V·s)], ε'_w is the real permittivity of water, and ϑ is the thickness of the diffuse double layer. The ionic mobility in the diffuse part of the double layer, several monolayers away from the surface, is

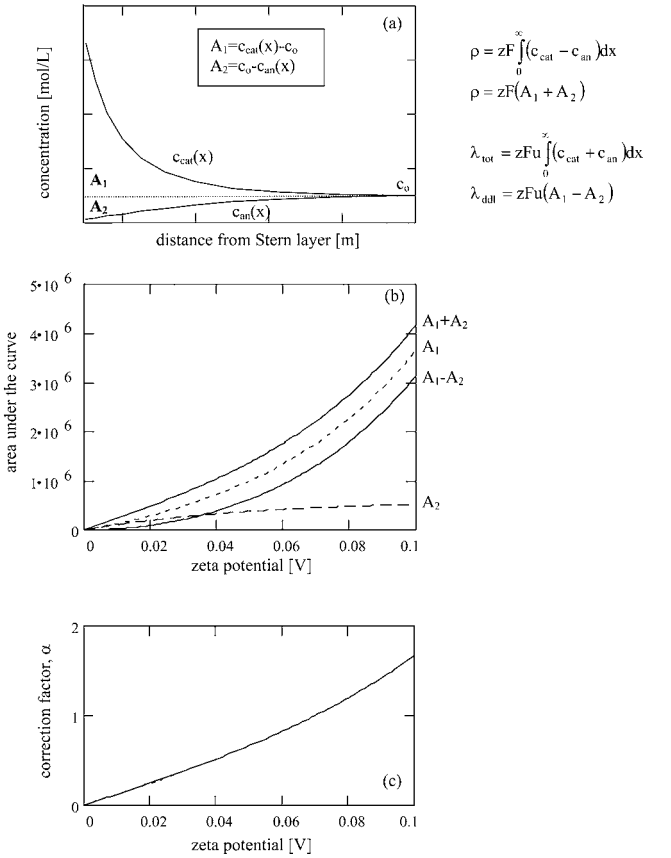

Figure 5. (a) Surface charge density ρ and excess surface conduction in the double layer λ_{ddl} as a function of ionic distribution in the diffuse double layer. (b) Variation of areas A_1, A_2, $(A_1 - A_2)$, and $(A_1 + A_2)$ with zeta potential ζ. (c) Correction factor for surface conduction when λ_{ddl} is estimated as shown in Eq. 14 (applies to NaCl).

presumed to be the same as in the bulk electrolyte (the fluid viscosity in adsorbed layers in discussed by Israelachvili, 1992). Eq. 13 assumes that the anionic deficit in the diffuse double layer is zero. The corrected surface conduction can be computed from the estimated value as

$$\lambda_{ddl} = \alpha\lambda_{ddl(est)} \tag{14}$$

where α is a correction factor that takes into consideration the true cationic and anionic distributions in the diffuse double layer with respect to the assumed distribution (Fig. 5a). Surface conduction λ_{ddl} depends on the concentration of excess cations (area A_1) and the deficit of anions (area A_2). It is important to realize that while the zeta potential ζ and the surface charge density ρ are functions of $(A_1 + A_2)$, excess surface conduction λ_{ddl} is a function of $(A_1 - A_2)$; analytical results are shown in Fig. 5a. The area A_1 increases exponentially with increasing zeta potential, while the area A_2 reaches a limiting value (Fig. 5b; see also Lyklema, 1995). The computed variation of $(A_1 - A_2)$ and $(A_1 + A_2)$ with zeta potential is also shown in Fig. 5b. In the case of a particle-water-NaCl electrolyte mixture, the ratio of the true and estimated surface conduction values α as a function of zeta potential ζ is shown in Fig. 5c. This correction factor takes into consideration the simplifying assumptions in both Eqs. 12 and 13.

Finally, an expression for the mixture conductivity is obtained by combining Eqs. 12, 13 and 14 and substituting into Eq. 11,

$$(\sigma_{mix})_{//} = \frac{\sigma_p + \sigma_{el}e + \alpha\left(\frac{\gamma_p}{g}\frac{\varepsilon'_w\Phi}{\vartheta}u_{cat}\right)S_a}{1+e} \tag{15}$$

In general, mineral particles have very low conductivity relative to the conductivity of electrolytes $\sigma_p \ll \sigma_{el}$ (in fact, the conductivity in particles is primarily based on electron movement rather than ionic movement as in electrolytes; hence, particle-electrolyte conductivity may develop to the extent that interfacial reactions may take place). Disregarding particle conductivity, Eq. 15 becomes

$$\sigma_{mix} = n\sigma_{el} + (1-n)\left(\alpha\frac{\gamma_p}{g}\frac{\varepsilon'_w\Phi}{\vartheta}u_{cat}\right)S_a \tag{16}$$

Therefore, the contribution of the electrolyte is restricted by the porosity of the medium $n = e/(1 + e)$, which is the volume of voids relative to the total volume. Equation 16 highlights that the reduction in conductivity due to the presence of non-conductive particles may be compensated by surface conduction. (The model by Grosse (1988) for spherical particles in asymmetric electrolytes predicts similar trends for mixture conductivity as a function of electrolyte conductivity.) In particular, Eq. 16 predicts that the mixture conductivity is greater than the electrolyte conductivity $\sigma_{mix}/\sigma_{el} > 1$ when

$$\alpha\frac{\gamma_p}{g}\frac{\varepsilon'_w\Phi}{\vartheta}u_{cat}\frac{S_a}{\sigma_{el}} > 1 \tag{17}$$

Therefore, the conductivity of the mixture is greater than the conductivity of the electrolyte when the electrolyte conductivity is low and particles have high specific surface.

Surface Conduction: Experimental Study

An experimental study was designed to assess the interplay between electrolyte conductivity and the contribution of surface conduction to the overall conductivity of the mixture. The kaolinite used for this study was Wilkay RP-2 kaolin (properties summarized in Table 1). High porosity mixtures were created using settlement tests conducted in a Plexiglas column (length = 120 cm, diameter = 3.7 cm), and complex dielectric permittivity measurements were obtained at the base of the column during

Table 1. Properties of tested materials.

Wilkay RP-2 Kaolin	
Producer: Wilkinson Kaolin Associates, Gordon, GA	
Sieve analysis[1]	
% passing #200 sieve	99
coefficient of uniformity, C_u	9.0
coefficient of curvature, C_c	0.67
median particle diameter, d_{50}	$3.6 \cdot 10^{-7}$ m
Specific surface [m^2/g][5]	21.9
Specific gravity[1]	2.6
GE Brightness, % Average[1]	78
pH (28% solids), Average[1]	5.2
Oil absorption, g/100 g clay[1]	40
Minimum dispersed viscosity, 62% solids[1]	4000+ cps
Raw colour[1]	Cream
Mica	
Producer: Franklin Industrial Minerals, Kings Mountain, NC	
Sieve analysis[1]	
% retained on 20 mesh (0.85 mm)	0.3
% retained on 40 mesh (0.425 mm)	78
% retained on 70 mesh (0.212 mm)	96
Average particle thickness, t_p[2]	≈0.125 mm
Average particle length, L_p[2]	≈1 mm
Bulk density [kg/m^3][1]	674
pH[1]	6.9
Specific gravity[1]	2.82
Hardness [Moh's][1]	2.50
Real relative dielectric permittivity (dry), κ'_p[3]	4
Conductivity (dry), σ_p[3]	10^{-4} S/m
Specific surface [m^2/g]	0.007[2] 0.215[4]

[1] Data provided by the manufacturer.
[2] Optical determination.
[3] High frequency dielectric permittivity and conductivity data were obtained using a HP-8752A network analyzer in conjunction with a HP-85070A dielectric coaxial termination probe (frequency = 20 MHz to 1.3 GHz).
[4] Gas adsorption measurement (Coulter SA 3100 Surface Area Analyzer).
[5] Gas adsorption measurement (Quantachrome NOVA 1200 Gas Sorption Analyzer).

settlement. The lower porosity mixtures were formed by mixing the kaolinite with the selected electrolyte at predetermined water contents (100% fluid saturation is maintained in both cases). All permittivity measurements were performed using a HP-8752A network analyzer in conjunction with a HP-85070A dielectric coaxial termination probe. The network analyzer was controlled by computer software that measures the complex reflection coefficient at the probe-specimen interface and computes the complex dielectric permittivity. Additional details can be found in Klein (1999).

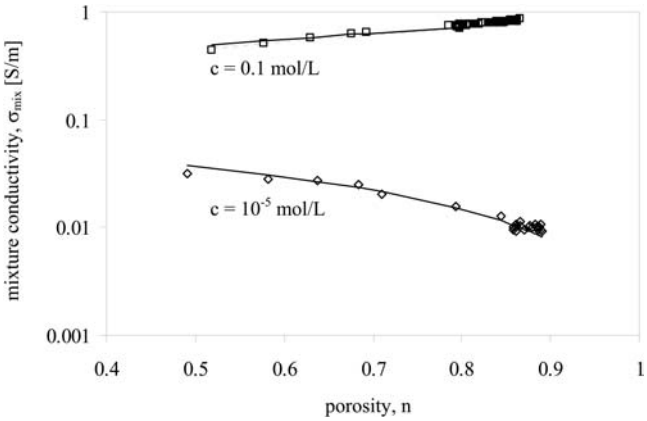

Figure 6. Conductivity of kaolinite-NaCl electrolyte slurries, for two ionic concentrations c, as a function of mixture porosity n. Conductivity values are measured using a HP-85070A coaxial termination probe (frequency = 0.1 GHz). Data (shown as points) are modeled using Eq. 11 with S_a = 21.9 m^2/g and $\lambda_{ddl} = 1.4 \cdot 10^{-9}$ S for both specimens (model shown as continuous line). The dashed line is Archie's equation (Eq. 19) with a = 1 and m = 1.

Experimental results and the fitting with Eq. 11 are shown in Fig. 6. These results confirm that the presence of the mineral particles renders a mixture with lower conductivity than σ_{el} in high concentration electrolytes, while the mixture conductivity σ_{mix} increases when kaolinite is added to low concentration electrolytes (data showing this behavior can also be found in Blewett *et al.,* 2001). As predicted by the model, the contribution of surface conduction and high specific surface to the conductivity of the mixture overcompensates for the reduced contribution of electrolyte conductivity due to the presence of particles $n\sigma_{el}$. The inverted surface conduction for both specimens is $\lambda_{ddl} = 1.4 \cdot 10^{-9}$ S. Revil and Glover (1997) presented a model which predicts that surface conduction for a quartz-electrolyte system varies from $1 \cdot 10^{-9}$ S to $4 \cdot 10^{-9}$ S as the concentration increases from 10^{-5} mol/L to 0.1 mol/L for pH = 7. Their model also predicts that surface conduction decreases as pH decreases, and that the magnitude of the increase in surface conduction with increasing ionic concentration decreases as pH decreases.

Discussion

Surface conduction was already considered in the early work by O'Konski (1960), Schwarz (1962), and Schurr (1964). Initial hypotheses assumed that ions in the

diffuse part of the double layer contribute to surface conduction, but that ions in the Stern layer do not (see for example Revil and Glover, 1997). Later results have shown that ions within the slip plane, which include ions in the Stern layer, can also contribute to surface conduction (Kijlstra *et al.,* 1992, 1993; Ennis and White, 1996; Mangelsdorf and White, 1998; Revil and co-workers, 1998, 1999; Lyklema, 2001). The contribution of inner and outer-sphere complexes in the Stern layer is time-scale dependent. Their mobility is restricted by the electrical potential wells associated with surface charges on the minerals. Therefore, their displacement is bound at low frequencies below the Stern layer polarization frequency, yet they can freely follow high frequency fields and fully contribute to global conduction.

When the specific surface is very small, as in the case of large particles, the mixture conductivity becomes

$$(\sigma_{mix})_{//} = \sigma_{el} n = \sigma_{el} \frac{e}{1+e} \tag{18}$$

Multiple internal scales, particle geometry, unsaturation, fabric, and tortuosity in conduction paths within real particulate materials restrict the accuracy of Eq. 18. These factors are taken into consideration in the empirical equation proposed by Archie (1942), which resembles Eq. 18

$$\sigma_{mix} = a\sigma_{el} n^m \tag{19}$$

The empirical coefficients 'a' and 'm' are used to match experimental data. In general, 'a' varies between 0 and 1, while 'm' varies between 1.4 and 2. This simple empirical equation can be conveniently fitted to most experimental data. For the 0.1 mol/L conductivity data shown in Fig. 6, the computed cementation factor is $m = 1$, suggesting negligible tortuosity in these specimens (saturated material, $a = 1$). Bussian (1983) relates Archie's cementation factor 'm' to the depolarization factor 'd' in the Hanai-Bruggeman equation

$$\frac{\sigma_{mix} - \sigma_{ddl}}{\sigma_{el} - \sigma_{ddl}} \left(\frac{\sigma_{el}}{\sigma_{mix}}\right)^d = n \tag{20}$$

where

$$m = (1-d)^{-1} \tag{21}$$

Using Eq. 21, the depolarization factor for the 0.1 mol/L mixtures is $d=0$. A depolarization factor of $d=0$ corresponds to infinitely long cylindrical rods with axes parallel to the electric field (Bussian, 1983), which means that polarization will not occur due to a lack of interfaces. Since the analytical derivation presented in this paper assumes infinitely long, parallel particles and continuous paths, such a model is a better approximation for the effective conductivity measured at frequencies above the frequency for spatial polarization (which is the case for the data shown in Fig. 6). At high frequencies, ionic displacement is small and it is less likely to be affected by the presence of boundaries, such as transverse particles or edges.

The inherent trade-off between surface conduction (low n) and electrolyte contribution (high n) in Eq. 16 is not captured in Archie's equation. Therefore fitting Eq. 19 to the low conductivity specimen data (10^{-5} mol/L) is misleading as these data show an increase in mixture conductivity with decreasing porosity.

If the field is normal to the particles, the effective conductivity of the pore fluid is also enhanced by the presence of the double layer. Assuming a series model,

$$(\sigma_{fluid})_{\perp} = t_w \left[\frac{t_w - \vartheta}{\sigma_{el}} + \frac{\vartheta}{(\sigma_{ddl})_{\perp}}\right]^{-1} \tag{22}$$

Given the variation of ionic concentration normal to the clay surface, the total conductivity contribution from the diffuse double layer normal to the clay surface $(\sigma_{ddl})_{\perp}$ is computed as the inverse of the integral of $dx/\sigma(x)$. The effectiveness of normal conduction is limited by the conductivity of the particle and the ensuing interfacial polarization. Hence, $(\sigma_{mix})_{\perp}$ is frequency dependent, as discussed next.

Fabric and Electrical Conductivity Anisotropy

The electrical conductivity of two-phase mixtures is a function of the electrical properties of both phases, as well as the volume fraction, size, shape, and orientation of inclusions. Electrically isotropic mixtures have the same electrical conductivity in all directions. However, highly anisotropic media, such as a conductive host medium containing platy inclusions, exhibits anisotropic electrical conductivity in relation to the orientation of the particles with respect to the electric field. Examples of materials that exhibit electrical anisotropy include clays (Mitchell and Arulanandan, 1968; Meegoda and Arulanandan, 1986), shales (Kunz and Moran, 1958), rocks (Hill, 1972; al Hagrey, 1994), sand-mica mixtures (Winkelmolen, 1972), meat (Bodakian and Hart, 1994), and semiconductors (Pal and Bose, 1996). Similar to electrical parameters, the compressibility, shear strength, and hydraulic conductivity of soils can be anisotropic (see for example Ohta and Nishihara, 1985; Al-Tabbaa and Wood, 1987; Leroueil *et al.,* 1990; Kirkgard and Lade, 1991; Little *et al.,* 1992; Sivakugan *et al.,* 1993; Anandarajah *et al.,* 1996; Anandarajah, 1997). Some of the underlying causal mechanisms are shared; thus, electrical conductivity anisotropy provides valuable information.

Anisotropy in the effective electrical conductivity σ_{eff} reflects not only anisotropy in the pore structure (pore fluid conduction) and in particle alignment (surface conduction), but double layer and spatial polarization losses, which are also affected by the soil fabric (see Santamarina *et al.,* 2001 for details). This section starts by addressing the extent

of electrical anisotropy that a soil can reach, and then a specially designed experimental study is undertaken.

Analytical Models – Extreme Values

The sensitivity of electrical conductivity to phase orientation (mixture anisotropy) can be illustrated for the extreme case of a material composed of two infinitely long layers. An upper bound exists in the case that the interface is parallel to the applied electric field (Fig. 7a), while a lower bound is found if the interface between the two phases is perpendicular to the direction of the applied field (Fig. 7b). If surface conduction develops, a third phase is considered as shown in the previous section (Eq. 15). Table 2 presents the models for these extreme cases. The frequency dependence of the series model develops due to spatial polarization (*i.e.,* charge accumulation at the interface between the two materials), and it has a corresponding relaxation time τ. Table 2 also presents reduced equations for the high and low frequency conductivities of the series model, as well as simple expressions for material anisotropy.

In most cases, the contrast between σ_{el} and σ_p is greater than the contrast between ε'_{el} and ε'_p, and higher effective conductivity anisotropy is expected at low frequencies as compared to high frequencies. However, the opposite trend may occur if the pore fluid has very low ionic concentration and the medium has high specific surface, as surface conduction becomes important. In real soils, the expected degree of anisotropy should be much lower than predicted by these extreme-case models, given the fact that particles are finite and pores are interconnected in all directions.

Relationships for the conductivity and permittivity of multi-phase materials involving spherical and spheroidal particles have been developed for low volume fractions (non-interacting inclusions) and high volume fractions (*e.g.,* self-consistent approximation). The effect of particle orientation is addressed in the early works by Sillars (1937) and Fricke (1953). Models and comprehensive reviews can be found in van Beek (1967), de Loor (1968), Wang and Schmugge (1980), Sen *et al.* (1981), and Koelman and Kuijper (1997).

Anisotropy: Experimental Study

The purpose of these tests was to quantify the impact of particle orientation on electrical conductivity in a well-controlled environment, where proper particle alignment can be attained.

Specimens with extreme fabric anisotropy were prepared with mica flakes by slow pluviation of the flakes through the aqueous electrolyte. Given the platy shape of the mica flakes and their size, gravity rather than electrostatic forces controls deposition, and the prevailing particle alignment was with their major axis normal to gravity (slow pluviation). The properties of the mica flakes are summarized

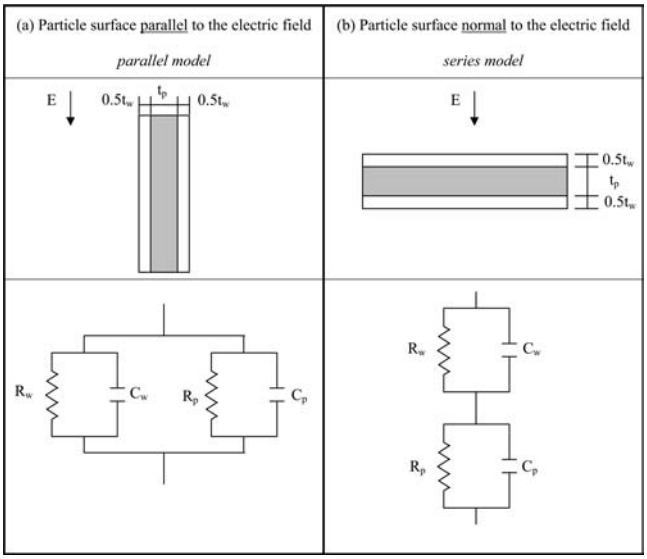

Figure 7. (a) Parallel and (b) series models for infinitely long platy particles with particle thickness t_p, surrounded by water with a water layer thickness $0.5t_w$. Note: the water layers can be modeled as a single layer of thickness t_w.

in Table 1. Two pore fluids were selected, deionized water to enhance the presence of surface conduction, and a c = 0.001 mol/L sodium chloride solution to minimize the importance of surface conduction. The mica particles were washed repeatedly in the corresponding fluid to remove excess ions and to form homoionic mixtures.

The specimen holder was designed to facilitate the preparation of specimens with particle alignment parallel and normal to the electrodes. The prismatic capacitor-type cell had a 45.7 cm^2 cross-sectional area and a thickness of 0.96 cm (Fig. 8). The faces of the cell consisted of stainless steel electrodes and the edges were made of Plexiglas strips. Specimens were prepared by positioning the cell either horizontally or vertically, removing the face that was at the top for the given alignment, filling the cell with the selected fluid, and slowly pluviating the mica flakes into the cell. Two-terminal electrical measurements were performed using a HP-4192A Low Frequency Impedance Analyzer.

Effective conductivity data from 10^4 Hz to 10^6 Hz are shown in Fig. 9 for the two fluids and the four mixtures. The upper (parallel) and lower (series) bounds from the analytical models given in Table 2 are also shown on this plot. Table 3 presents the model parameters. The following observations can be made:

- The effective conductivity of the specimen with particles oriented parallel to the applied field is greater than the σ_{eff} of the specimen with particles perpendicular to the applied field for both ionic concentrations.

Table 2. Analytical models-extreme values.

	Parallel	Series
Mixture conductivity	$(\sigma_{mix})_{//} = n\sigma_{el} + (1-n)\sigma_p$	$(\sigma_{mix})_{\perp} = -\omega\ \mathrm{Im}(\varepsilon^*_{mix}) = -\omega\ \mathrm{Im}\left[\left(\frac{n}{\varepsilon^*_{el}} + \frac{1-n}{\varepsilon^*_{p}}\right)^{-1}\right]$
Relaxation time	none	$\tau = \frac{\kappa'_p n + \kappa'_{el}(1-n)}{\sigma_p n + \sigma_{el}(1-n)}$
Low frequency limit	n/a	$(\sigma_{mix\perp})_{low\,f} = \left[\frac{n}{\sigma_{el}} + \frac{(1-n)}{\sigma_p}\right]^{-1}$
High frequency limit	n/a	$(\sigma_{mix\perp})_{high\,f} = \frac{n\sigma_{el}\kappa'^2_p + (1-n)\sigma_p\kappa'^2_{el}}{[n\kappa'_p + (1-n)\kappa'_{el}]^2}$
Low frequency anisotropy	$\frac{(\sigma_{mix})_{//}}{(\sigma_{mix})_{\perp}} \approx n(1-n)\frac{\sigma_{el}}{\sigma_p}$	
High frequency anisotropy	$\frac{(\sigma_{mix})_{//}}{(\sigma_{mix})_{\perp}} \approx \left[n + (1-n)\frac{\varepsilon'_{el}}{\varepsilon'_p}\right]^2$	

Notation: σ is conductivity; subscripts el, p, and mix denote the electrolyte, particle and mixture, respectively; n is porosity; the permittivity is $\varepsilon^* = \varepsilon' - j$, (σ/ω); ω is frequency; $j^2 = -1$ denotes an imaginary number; τ is the relaxation time; $\kappa' = \varepsilon'/\varepsilon_o$ is the real relative permittivity; $\varepsilon_o = 8.85 \cdot 10^{-12}$ F/m is the permittivity of free space.

- The effective conductivities of the mixtures with high ionic concentration (c = 0.001 mol/L) are less than the effective conductivity of the pure fluid, because the presence of the low conductivity mica flakes hinders conduction across the electrolyte. In this case, tortuosity plays a dominant role.
- However, the effective conductivities of the mixtures with deionized water are greater than the effective conductivity of the pure fluid, indicating that surface conduction gains relevance in the low ionic concentration specimens, as predicted in the previous section.
- The increase in effective conductivity at frequencies above approximately $10^{4.5}$ Hz suggests the presence of a relaxation. This increase is only slightly evident in the 0.001 mol/L specimens.
- The effective conductivity anisotropy is more pronounced for the high ionic concentration specimens: at 10^4 Hz, $(\sigma_{mix})_{//}/(\sigma_{mix})_{\perp} \approx 3$ in the specimens with sodium chloride, while $(\sigma_{mix})_{//}/(\sigma_{mix})_{\perp} \approx 1.8$ for the specimens prepared with deionized water. A small reduction in anisotropy with frequency is observed for the c = 0.001 mol/L solution; however, a small increase takes place when deionized water is used.
- Archie's cementation factors were calculated for the series (m = 4.3) and parallel (m = 1.5) high ionic concentration specimens at 10^4 Hz. Both cementation factors are greater than one, indicating that at these low frequencies, boundaries affect conductivity. The ratio of the cementation factors is $m_{\perp}/m_{//} \approx 3$, which is similar to ratio $(\sigma_{mix})_{//}/(\sigma_{mix})_{\perp}$. Archie's law cannot be adequately invoked for the low ionic concentration specimens due to surface conduction effects.

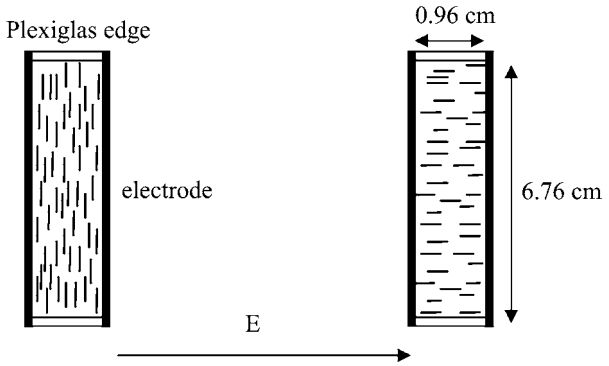

Figure 8. Specimen holder. Mica particles aligned perpendicular and parallel to the electric field E.

The data show that the electrical properties of these mixtures are a function of particle orientation and ionic concentration. While the series and parallel models capture

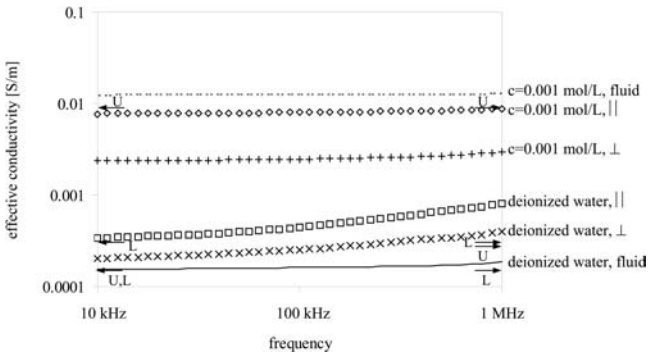

Figure 9. Effective conductivity data for mixtures of mica flakes with NaCl at two different ionic concentrations. Measurements were conducted with the mica flakes oriented parallel || and perpendicular ⊥ to the electric field. The upper U (parallel) and lower L (series) bounds from the analytical models presented in Table 2 are shown as arrows.

Table 3. Model parameters.

	deionized water	c = 0.001 mol/L
Real relative permittivity of water, κ'_w	78	
Real relative permittivity of mica, κ'_p	4	
Particle conductivity, σ_p	10^{-4} S/m	
Fluid conductivity, σ_{el}	$1.56 \cdot 10^{-4}$ S/m	$126 \cdot 10^{-4}$ S/m
Porosity, n (parallel)	0.73	0.73
Porosity, n (series)	0.71	0.68

these variables, they cannot adequately predict the measurements because important properties of the system are neglected, in particular, surface conduction must be included for low conductivity specimens and the connectivity of the pores through water layers on the sides of the particles must be modeled. At these lower frequencies, ionic displacement is larger and it is more likely to be affected by the presence of boundaries.

Final Comments and Conclusions

Effective conductivity data are minimally impacted by electrode effects at kHz frequencies and higher; therefore, conductivity measurements provide a robust means of evaluating soil specimens. Figure 10 schematically summarizes the main observations from this study. Salient conclusions follow.

Conductivity in wet soils reflects the contributions of the conductivity within particles, the bulk fluid conductivity, and the additional surface conduction due to the increased counterion concentration in the diffuse double layer around particles. At low potentials, the contribution of surface conduction is proportional to specific surface and the potential at the plane where the ions contribute to surface conduction.

Surface conduction makes a noticeable contribution to the global conductivity of mixtures with low ionic concentration fluids, while this contribution is negligible if the fluid has high ionic concentration.

Conductivity is a function of particle orientation. The effective conductivity is greatest in mixtures with pores preferentially oriented parallel to the electric field. Furthermore, the contribution of surface conduction to the conductivity of the soil is more significant when particles are oriented parallel to the field. In mixtures where surface conduction effects are significant, the application of Archie's law may be misleading.

The electrical conductivity anisotropy in real soils is smaller than the extreme anisotropy predicted using two-layer models because of the multidirectional connectivity of the internal porosity. In fact, while the specimens in this study were designed to attain very high anisotropy, the measured conductivity anisotropy varied between 1.8 and 3 (for deionized water and the 0.001 mol/L solution, respectively). In most geo-environments, the level of conductivity anisotropy should be expected to decrease with increasing frequency at frequencies above the spatial polarization frequency. The anisotropy in conductivity at low frequencies increases with increasing relative fluid-particle conductivity σ_{el}/σ_p. On the other hand, the high frequency conductivity anisotropy increases with the permittivity ratio $\varepsilon'_{el}/\varepsilon'_p$.

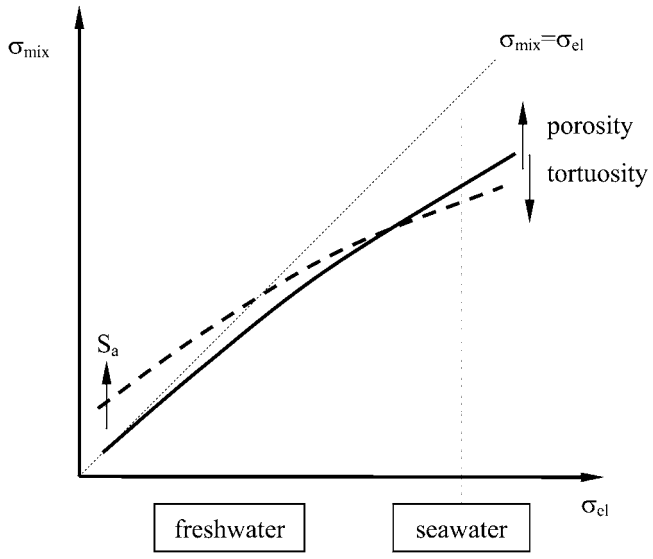

Figure 10. The electrical conductivity of soils—Summary. The continuous line is a more typical trend for sands, while the dashed line corresponds to clays. The conductivity of the soil σ_{mix} is determined by the conductivity of the electrolyte that makes the pore fluid σ_{el}, but it is reduced by the porosity n of the soil. Tortuosity also hinders conduction, particularly at low frequencies; clays may exhibit higher tortuosity than sands. The contribution of surface conduction is most relevant at low electrolyte conductivity and is proportional to the specific surface of the soil S_a.

Acknowledgments

Support for this research was provided by the National Science Foundation and the Georgia Mining Industry.

References

Adamson, A.W., 1990, Physical chemistry of surfaces, 5th ed.: John Wiley & Sons, Inc., New York.

al Hagrey, S.A., 1994, Electrical study of fracture anisotropy at Falkenberg, Germany: Geophysics, **59**, 881–888.

Al-Tabbaa, A., and Wood, D.M., 1987, Some measurements of the permeability of kaolin: Géotechnique, **37**, 499–503.

Anandarajah, A., Kuganenthira, N., and Zhao, D., 1996, Variation of fabric anisotropy of kaolinite in triaxial loading: Journal of Geotechnical Engineering, **122**, 633–640.

Anandarajah, A., 1997, Influence of particle orientation on one-dimensional compression of montmorillonite: Journal of Colloid and Interface Science, **194**, 44–52.

Annan, A.P., 1992, Ground penetrating radar workshop notes: Sensors and Software, Mississauga.

Archie, G.E., 1942, The electrical resistivity log as an aid in determining some reservoir characrteristics: Transactions of the American Institute of Mining, Metallurgical, and Petroleum Engineers, **146**, 54–62.

Blewett, J., McCarter, W.J., Chrisp, T.M., and Starrs, G., 2001, Monitoring sedimentation of a clay slurry: Géotechnique, **51**, 723–728.

Bodakian, B., and Hart, F.X., 1994, The dielectric properties of meat: IEEE Transactions on Dielectric and Electrical Insulation, **1**, 181–187.

Bussian, A.E., 1983, Electrical conductance in a porous medium: Geophysics, **48**, 1258–1268.

Daniels, J.J., and Roberts, R.L., 1994, Ground penetrating radar for geotechnical applications: *in* Geophysical characterization of sites, Woods, R.D. (ed.), Oxford & IBH Publishing Co. Pvt. Ltd., New Delhi, 1–13.

de Loor, G.P., 1968, Dielectric properties of heterogeneous mixtures containing water: The Journal of Microwave Power, **3-2**, 67–73.

Edwards, R.N., and Nabighian, M.N., 1991, The magnetometric resistivity method: Electromagnetic methods in applied geophysics, Volume 2, application, Parts A and B: *in* Investigations in Geophysics No. 3, Nabighian, M. (ed.), Society of Exploration Geophysics, Tulsa, Oklahoma, 47–104.

Ennis, J., and White, L.R., 1996, Dynamic Stern layer contribution to the frequency-dependent mobility of a spherical colloid particle: A low-zeta-potential analytic solution: Journal of Colloid and Interface Science, **178**, 446–459.

Fricke, H., 1953, The Maxwell-Wagner dispersion in a suspension of ellipsoids: Journal of Physical Chemistry, **57**, 934–937.

Grosse, C., 1988, Permittivity of a suspension of charged spherical particles in electrolyte solution. 2: Influence of the surface conductivity and asymmetry of the electrolyte on the low- and high-frequency relaxations: Journal of Physical Chemistry, **92**, 3905–3910.

Hill, D.G., 1972, A laboratory investigation of electrical anisotropy in Precambrian rocks: Geophysics, **37**, 1022–1038.

Israelachvili, J., 1992, Intermolecular and surface forces, 2nd ed.: Academic Press, New York.

Keller, G.V., and Frischknecht, F.C., 1966, Electrical methods in geophysical prospecting: Pergamon Press, New York.

Kijlstra, J., van Leeuwen, H.P., and Lyklema, J., 1992, Effects of surface conduction on the electrokinetic properties of colloids: Journal of the Chemical Society Faraday Transactions, **88**, 3441–3449.

Kijlstra, J., van Leeuwen, H.P., and Lyklema, J., 1993, Low-frequency dielectric relaxation of hematite and silica sols: Langmuir, **9**, 1625–1633.

Kirkgard, M.M., and Lade, P.V., 1991, Anisotropy of normally consolidated San Francisco Bay mud: ASTM Geotechnical Testing Journal, **14**, 231–246.

Klein, K., 1999, Electromagnetic properties of high specific surface minerals: (Ph.D. thesis), Georgia Institute of Technology, Atlanta, Georgia.

Klein, K., and Santamarina, J.C., 1997, Methods for broad-band dielectric permittivity measurements (soil-water mixtures, 5 Hz to 1.3 GHz): ASTM Geotechnical Testing Journal, **20**, 168–178.

Klein, K., and Santamarina, J.C., 2000, Ferromagnetic inclusions in geomaterials: Implications on electromagnetic measurements: Journal of Geotechnical and Geoenvironmental Engineering, **126**, 167–179.

Koelman, J.M.V.A., and de Kuijper, A., 1997, An effective medium model for the electric conductivity of an N-component anisotropic and percolating mixture: Physica A, **247**, 10–22.

Kunz, K.S., and Moran, J.H., 1958, Some effects of formation anisotropy on resistivity measurements in boreholes: Geophysics, **XXIII**, 770–794.

Leroueil, S., Bouclin, G., Tavenas, F., Bergeron, L., and La Rochelle, P., 1990, Permeability anisotropy of natural clays as a function of strain: Canadian Geotechnical Journal, **27**, 568–579.

Little, J.A., Muir Wood, D., Paul, M.A., and Bouazza, A., 1992, Some laboratory measurements of permeability of Bothkennar clay in relation to soil fabric: Géotechnique, **42**, 355–361.

Lyklema, J., 1991, Fundamentals of interface and colloid science volume I: Fundamentals: Academic Press, New York.

Lyklema, J., 1995, Fundamentals of interface and colloid science volume II: Solid-liquid interfaces: Academic Press, New York.

Lyklema, J., 2001, Surface conduction: Journal of Physics: Condensed Matter, **13**, 5027–5034.

Mangelsdorf, C.S., and White, L.R., 1998, The dynamic double layer—Part 1 theory of a mobile stern layer: Journal of the Chemical Society Faraday Transactions, **94**, 2441–2452.

Marshall, D.J., and Madden, T.R., 1959, Induced polarization, A study of its causes: Geophysics, **24**, 790–816.

Meegoda, N.J., and Arulanandan, K., 1986, Electrical method of predicting in situ stress state of normally consolidated clays: *in* Use of in situ tests in geotechnical engineering: Proceedings of In Situ '86, Geotechnical Special Publication No. 6, ASCE, NY, 794–808.

Mitchell, J.K., and Arulanandan, K., 1968, Electrical dispersion in relation to soil structure: Journal of the Soil Mechanics and Foundations Division: In Proceedings of the ASCE, **SM 2**, 5853–471

Ohta, H., and Nishihara, A., 1985, Anisotropy of undrained shear strength of clays under axi-symmetric loading conditions: Soils and Foundations, Japanese Society of Soil Mechanics and Foundation Engineering, **25**, 73–86.

O'Konski, C.T., 1960, Electrical properties of macromolecules. V. Theory of ionic polarization in polyelectrolytes: Journal of Physical Chemistry, **64**, 605–618.

Pal, S., and Bose, D.N., 1996, Growth, characterisation and electrical anisotropy in layered chalcogenides GaTe and InTe in Solid State Communications, **97**, 725–729.

Revil, A., and Glover, P.W.J., 1997, "Theory of ionic-surface electrical conduction in porous media": Physical Review B, **55**, 1757–1773.

Revil, A., and Glover, P.W.J., 1998, Nature of surface electrical conductivity in natural sands, sandstones, and clays: Geophysical Research Letters, **25**, 691–694.

Revil, A., Pezard, P.A., and Glover, P.W.J., 1999, Streaming potential in porous media—1. Theory of the zeta potential: Journal of Geophysical Research, **104**, 20021–20031.

Santamarina, J.C., Klein, K.A., and Fam, M.A., 2001, Soils and waves: John Wiley & Sons, Toronto.

Schurr, J.M., 1964, On the theory of the dielectric dispersion of spherical colloidal particles in electrolyte solution: Journal of Physical Chemistry, **68**, 2407–2413.

Schwarz, G., 1962, A theory of the low-frequency dielectric dispersion of colloidal particles in electrolyte solution: Journal of Physical Chemistry, **66**, 2636–2642.

Sen, P.N., Scalla, C., and Cohen, M.H., 1981, A self-similar model for sedimentary rocks with application to the dielectric constant of fused glass beads: Geophysics, **46**, 781–795.

Sillars, B.A., 1937, The properties of a dielectric containing semiconductivity particle of various shapes: Journal of the Institute of Electrical Engineers, **80**, 378–394.

Sivakugan, N., Chameau, J.L., and Holtz, R.D., 1993, Anisotropy studies on cuboidal shear device: Journal of Geotechnical Engineering, **119**, 973–983.

Stumm, W., 1992, Chemistry of the solid-water interface: John Wiley & Sons, Inc., New York.

Topp, G.C., Davis, J.L., Bailey, W.G., and Zebchuk, W.D., 1984, The measurement of soil water content using a portable TDR hand probe: Canadian Journal of Soil Science, **64**, 313–321.

van Beek, L.K.H., 1967, Dielectric behaviour of heterogeneous systems: Progress in Dielectrics, **7**, London Heywood Books.

Velde, B., 1992, Introduction to clay minerals—Chemistry, origins, uses and environmental significance: Chapman and Hall, New York.

Wang, J.R., and Schmugge, T.J., 1980, An empirical model for the complex dielectric permittivity of soil as a function of water content: IEEE Transactions on Geoscience and Remote Sensing, **GE-18**, 288–295.

Ward, S.H., 1990, Resistivity and induced polarization methods: In Geotechnical and environmental geophysics, Volume I: review and tutorial, investigations in geophysics No. 5, Ward, S. (ed.), Society of Exploration Geophysics, Tulsa, Oklahoma, pp. 147–189.

Weaver, C. E., 1989, Clays, muds, and shales: Elsevier, New York.

Winkelmolen, A.M., 1972, Dielectric anisotropy and grain orientation: The American Association of Petroleum Geologists Bulletin, **56**, 2150–2159.